Indian Journal of Fundamental and Applied Life Sciences ISSN: 2231– 6345 (Online)
An Open Access, Online International Journal Available at www.cibtech.org/sp.ed/jls/2016/02/jls.htm
2016 Vol. 6 (S2), pp. 555-564/Shahpar
Research Article

NUMERICAL AND EXPERIMENTAL ANALYSIS TO EXACTLY PREDICT THE CRACK BY THE DYNAMIC FORMING LIMIT CRITERIA IN LASER ASSISTED FORMING PROCESS OF SHEET METAL

***Majid Lotfi Shahpar**
Department of Science in Mechanical Engineering, Jam Petrochemical Company, Pars Special Economic Energy Zone, Assaluyeh, Boushehr, Iran
**Author for Correspondence*

ABSTRACT
In current article, strain rate effect using dynamic forming limit diagram in forming process of sheet metal stainless steel 316 using laser is studied. This break criterion is based on Marciniak and Kuczynski model and solving equations is down by Newton Raphson method. To compare dynamic and static forming limit diagram, first it is simulated in Abaqus finite element software, then experimental test is done by the laser and results are compared. We conclude that in laser assisted forming process that strain rate effects on material behavior, the only exact criterion to predict crack is dynamic forming limit.

Keywords: *Strain Rate, Dynamic Forming Limit, Laser Assisted Forming*

INTRODUCTION
Using forming limit diagrams is an appropriate method to predict configurability of sheet metal that in fact is indicative of change in shape under different loadings. Forming limit diagram is a useful tool to determine forming sheet metal in laser assisted forming process. Developing usage of forming limit diagram as a powerful tool is impressive to practical and scientific evaluating of ductile sheet. This diagram shows the maximum main strain to the minimum main strain which the sheet can tolerate it to the threshold of localized necking. This rate of strain that is tolerated by the sheet before localized necking is called limit strain. Forming limit diagram shows rate of maximum limit strain in different loadings. Theory of forming limit diagram is raised for the first time by Keeler (1965) and Goodwin (1969). Marciniak and Kuczynski (1967) and Marciniak *et al.*, (1973) developed it and created a model that is able to predict localized necking. They concluded that break in sheet is not occurred suddenly but also non-uniformity and in inhomogeneous in aggregate material cause localized thinness and finally break. This inhomogeneous is considered as a track that divides the sheet surface to two parts: inhomogeneous and inhomogeneous. Several researchers studied different effects of factor on forming limit diagram using this model. Barata *et al.*, (1984) studied effects of linear and nonlinear loadings on anisotropic sheets and they concluded that theory of track perpendicular to the main axis for non-anisotropic material is not valid. Sowerby and Duncant (1971) studied effects of mechanical properties like symbol of strain hardening and limit elastic strain on the right part of the forming limit diagram and come to this conclusion that as symbol of strain hardening and limit elastic strain on increase, right part of the forming limit diagram increase. Moshksar and Mansorzadeh (2003) studied forming limit diagram AL3105. They checked out effects of lubrication on break and they concluded that if lubrication is appropriate, forming will be more appropriate and time of break will be delayed. Campos *et al.*, (2006) studied both experimentally and numerically forming limit diagram stainless steel AIAI304 and they concluded that forming limit diagram of AL littlie depends on strain rate. Ahmadi *et al.*, (2009) achieved forming limit diagram for three different metal types using experimental and theoretical method and concluded that increasing hardening strain symbol increase diagram surface although increasing vertical anisotropy coefficient decreases right part of forming limit diagram and increases left part of it. Kim *et al.*, (2011) studied strain rate effects on forming limit criteria of CQ metal and proved doing experiment in different directions relative to rolling that this material depends on strain rate. In current experiment,

three forming limit diagram are calculated numerically: forming limit diagram independent to strain rate, forming limit diagram depend to strain rate, dynamic forming limit diagram.

Marciniak and Kuczynski Model (M-K Model)

In current article, damage criteria depends on achieving limit strains is based on M-K model. In this model, a narrow track is considered on the sheet surface so that sheet is divided to homogeneous part and inhomogeneous part (track) that is shown by a and b symbols, respectively. Figure 1 shows existence of track in this model. To modeling track, inhomogeneous coefficient is defined which is expressed in equation 1(Marciniak and Kuczynski, 1967).

$$f = \frac{t_b}{t_a} \qquad (1)$$

In equation 1, t_a and t_b are respectively sheet thickness in homogeneous and inhomogeneous parts. Limit strain are achieved when effective strain in inhomogeneous part to effective strain in homogeneous part ratio go more than 10 (Barata *et al.*, 1984). From balance equations in track direction, we have:

$F^a_{nt}=F^b_{nt}$ (2a) $F^a_{nn}=F^b_{nn}$ (2b)

Which in equation 2, F_{nn} and F_{nt} are forces in perpendicular to and tangent to track and per unit length. From relationship between tension and force in equation 3, we have:

$$\sigma^a_{nt}\exp(\varepsilon^a_3)t^a_0 = \sigma^b_{nt}\exp(\varepsilon^b_3)t^b_0 \qquad (3a)$$

$$\sigma^a_{nn}\exp(\varepsilon^a_3)t^a_0 = \sigma^b_{nn}\exp(\varepsilon^b_3)t^b_0 \qquad (3b)$$

Which in equation 3, σ_{nn} and σ_{nt} are components perpendicular and tangent to stress. t^a_o and t^b_o are primary thickness of homogeneous and inhomogeneous parts. ε_3 is strain along thickness that according to principle of material volume being constant, we have:

$$\varepsilon_3 = -(\varepsilon_1+\varepsilon_2) \qquad (4)$$

Equation 1 can be shown respect to primary inhomogeneous (Marciniak and Kuczynski, 1967).

$$f = f_0\exp(\varepsilon^b_3-\varepsilon^a_3) \qquad (5a)$$

Which in equation 5a:

$$f_0 = \frac{t^b_0}{t^a_0} \qquad (5b) \qquad t = t_0\exp(\varepsilon_3) \qquad (5c)$$

According to equation 3 and 5, we have:

$$f\sigma^b_{nn} = \sigma^a_{nn} \qquad (6a) \qquad f\sigma^b_{nt} = \sigma^a_{nt} \qquad (6b)$$

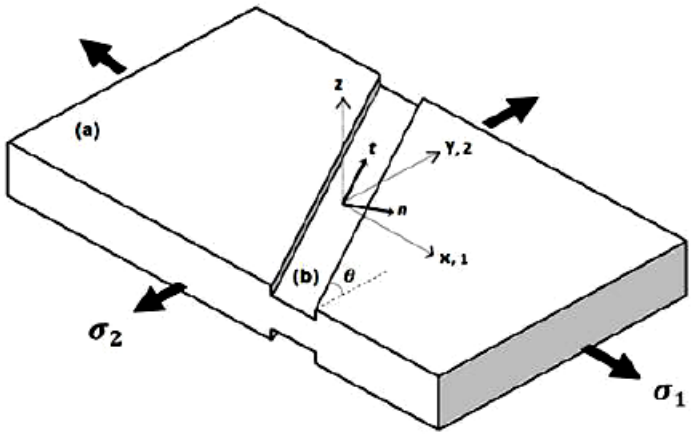

Figure 1: M-K Model and Assumption of Track Existence

Along to tangent to track, compatibility equation is as equation 7:

$$d\varepsilon_{tt}^{a} = d\varepsilon_{tt}^{b} \qquad (7)$$

Therefore, we can calculate all stress and strain components in homogeneous parts and other passive parameters are achieved using equations 1-7. Passive parameters are:

$\sigma_{nt}{}^{b}$ **and** $\sigma_{nn}{}^{b}$ **and** $\sigma_{tt}{}^{b}$ **and** $\overline{d\varepsilon}^{b}$

Solving Equation Numerically

To calculate limit strain, first we must get stress and strain components in homogeneous part. In this theory, ratio between stresses in homogeneous part throughout loading is constant. Also it's assumed in this equation, plane stress is established. This ratio in equation 8 is shown by symbol α. α is value between 0 and 1.

$$\alpha = \frac{\sigma_{22}}{\sigma_{11}} \qquad (8)$$

Effective Stress and strain are related under Swift equation (Hosford, 2007).

$$\bar{\sigma}_Y = K(\varepsilon_0 + \bar{\varepsilon})^n \dot{\varepsilon}^m \qquad (9)$$

Which in equation 9, $\bar{\sigma}_Y$ and $\bar{\varepsilon}$ are effective stress and strain, respectively, $\dot{\varepsilon}$ is strain rate, K, is strength coefficient, n is hardening strain symbol, m is power of sensitivity to strain rate, ε_o is limit elastic strain. To begin, growth of effective strain $\overline{d\varepsilon^a}$ is applied as 0.0004.

Hill yield criterion 1948 follows as equation 10a (Hosford, 2007):

$$\begin{aligned} 2f(\sigma) = [&G(\sigma_{22}-\sigma_{33})^2 + F(\sigma_{11}-\sigma_{33})^2 \\ &+ H(\sigma_{11}-\sigma_{22})^2 + 3\sigma_{31}{}^2 \\ &+ 3\sigma_{23}{}^2 + 3\sigma_{12}{}^2]^{1/2} \end{aligned} \qquad (10a)$$

Which in equation 10a, σ and $f(\sigma)$ are stress in different directions and yield function. Also F, G, H, L, M, N are inhomogeneous coefficients. In equation 10a, we have:

$$H = \frac{r_0}{r_0 + 1} \qquad (10b)$$

$$F = \frac{r_0}{(r_0 + 1)r_{90}} \qquad (10c)$$

$$G = \frac{1}{r_0 + 1} \qquad (10d)$$

Which in equation 10, r_o and r_{90} are inhomogeneous coefficient in different rolling and perpendicular to rolling direction, respectively. Assuming being plane of stress as well as being consistent of main axis and existing axis in sheet, equation 11 is made:

$$2f(\sigma) = \sqrt{G(\sigma_{22})^2 + F(\sigma_{11})^2 + H(\sigma_{11}-\sigma_{22})^2} \qquad (11)$$

Using equations 8 and 10, equations 12 are made:

$$\sigma_{11} = \frac{\bar{\sigma}_Y(r_{90}(r_0+1))}{\sqrt{r_{90} + r_0\alpha^2 + r_0 r_{90}(1-\alpha)^2}} \qquad (12a)$$

$$\sigma_{22} = \alpha\sigma_{11} \qquad (12b)$$

To achieving effective strains in homogenous part, flow rule is used which is expressed in equation (Hosford, 2007).

$$d\varepsilon_{ij} = d\lambda \frac{\partial f(\sigma)}{\partial \sigma_{ij}} \qquad (13a)$$

$$d\lambda = \frac{d\bar{\varepsilon}}{\bar{\sigma}} \qquad (13b)$$

According to equations 10, 11and 13, equations 14 are made:

$$q1=\frac{2r_{90}(\sigma_{11})+2r_0r_{90}(\sigma_{11}-\sigma_{22})}{2r_{90}(r_0+1)\bar{\sigma}_Y} \quad (14a)$$

$$q2=\frac{2r_{90}(\sigma_{11})-2r_0r_{90}(\sigma_{11}-\sigma_{22})}{2r_{90}(r_0+1)\bar{\sigma}_Y} \quad (14b)$$

Using equations 14, we can express main strains in homogenous part according to equation 15:

$$d\varepsilon_{11}=q1(d\bar{\varepsilon}) \quad (15a) \qquad d\varepsilon_{22}=q2(d\bar{\varepsilon}) \quad (15b)$$

All components of equation 15 are in main directions that being active of strain components in track is required rotation matrix is used as equation 16:

$$\sigma^{ntz}=T\sigma^{xyz}T^T=\begin{bmatrix}\sigma_{nn} & \sigma_{nt}\\ \sigma_{nt} & \sigma_{tt}\end{bmatrix} \quad (16a) \qquad T=\begin{bmatrix}\cos\theta & -\sin\theta\\ \sin\theta & \cos\theta\end{bmatrix} \quad (16b)$$

Angle θ, in equation 16b, is angle between along track and axis 2. From equation 17, we have (Sowerby and Duncant, 1971):

$$\tan(\theta+d\theta)=\frac{1+d\varepsilon_{11}^a}{1+d\varepsilon_{22}^a}\tan(\theta) \quad (17)$$

By achieving strain components in homogeneous part using equations 8-17, we can obtain passive components that are stress and strain of inhomogeneous part. If we show passive vector by X, then from equation 18, we have:

$$X=\left[\sigma_{nt}^b;\sigma_{nn}^b;\sigma_{tt}^b;d\bar{\varepsilon}^b\right] \quad (18)$$

In this theory, we assume that the moment of starting necking is the time when effective strain growth in inhomogeneous part gets 10 times effective strain growth in homogenous part (Barata *et al.*, 1984). It is interesting to note that per each α, we have maximum an answer. Algorithm of this application is written using FORTRAN programming language and resulting answers is derived from solution property by Newton-Raphson method.

Putting answers together per each strain ratio α, set of points are achieved that are given limit strains in forming limit diagram. Jie *et al.*, (2009) discussed numerical and experimental study of metal forming limit diagram.

Table 1 shows mechanical properties of metal. They used damage model by the name of vertex model and compared forming limit diagram resulting from vertex model and experimental method. They achieved forming limit diagram in strain rate of 4 seconds. Their results show that there is very little difference between two diagrams drawn from numerical and experimental method but method of this research is based on M-K model.

To study accuracy of written algorithm in current search, forming limit diagram for metal is obtained using M-K model and with regards to mechanical properties as table 1 and they compared with results of Jie *et al.*, (2009) that are obtained by the experimental method and vertex model as figure 2.

Table 1: Mechanical Properties of Stainless Steel 316 (Jie *et al.*, 2009)

Value	Mechanical Properties
0.2	Hardening Strain Symbol (n)
400	Strength Coefficient (k) Respect to MPa
0.05	Power of Sensitivity to Strain Rate (m)
0.0003	Limit Elastic Strain

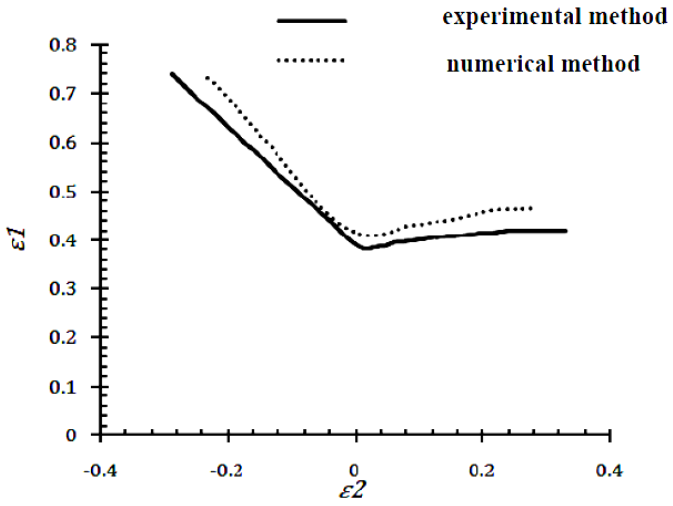

Figure 2: Comparing Forming Limit Diagram Resulting from M-K Model in Current Research and Forming Limit Diagram Resulting from Experimental Method in Jie *et al.*, (2009)

Forming Limit Diagram Independent to Strain Rate, Dependent to Strain Rate and Dynamic Forming Limit Diagram

Forming limit diagram depends on metal properties, entering mechanical properties as table 2 to the program which is written according to M-K algorithm, forming diagram of respected material is obtained. If sensitivity coefficient to strain rate is 0, in fact it means material has behavior independent to strain rate. In this way, equation 9 becomes equation 19:

$$\bar{\sigma}_Y = K(\varepsilon_0 + \bar{\varepsilon})^n \quad (19)$$

Figure 3 show both independent diagram to strain rate and depended diagram to strain rate. Depended diagram to strain rate in figure 9 is obtained in strain rate of 20 per second. Considering power of sensitivity to strain rate parameter, surface of forming limit diagram of metals is increased, since (Assempour and Ganjiani, 2008) concluded that increasing m causes increase in forming limit. In fact, parameter m causes that moment of starting localized thinness is delayed because surface of diagram is moved upward.

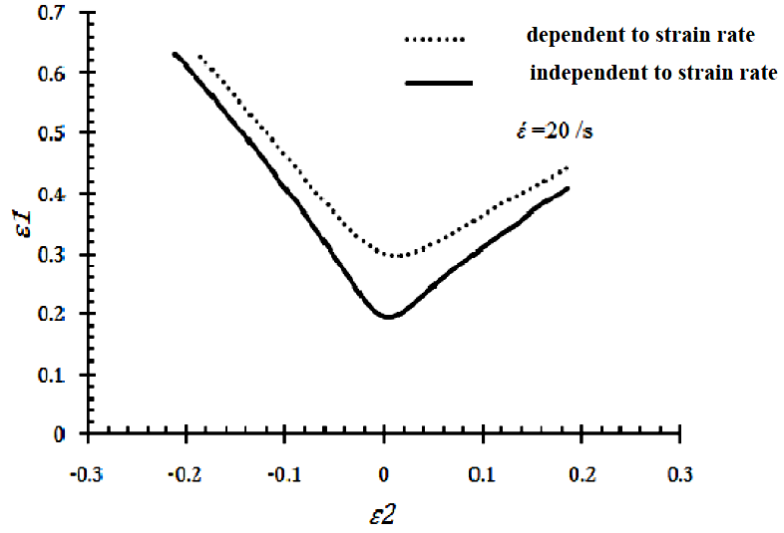

Figure 3: Independent and Dependent Forming Limit Diagram to Strain Rate of Stainless Steel 316

Table 2: Mechanical Properties of Stainless Steel 316 in Three Directions of Rolling

45º	90º	In Direction of Rolling	Position Respect to Rolling
0.2394	0.2356	0.2387	Hardening strain symbol (n)
654	643	650	Strength coefficient (k) respect to MPa
0.0178	0.0181	0.0187	Power of sensitivity to strain rate (m)
0.007	0.007	0.007	Limit elastic strain (ε_o)

Forming limit diagrams of stainless steel 316 are semi-static either dependent to strain rate or independent to strain rate because strain rate parameter is not included numerically in equation 9. Dynamic criterion in each strain rate determines forming limit. Entering numerical strain rate to equation 9 and its effect to other mentioned equations, dynamic forming limit diagram is calculated, quantity of strain rate is included in this criterion. Figure 4 shows dynamic forming limit diagram of stainless steel 316 in strain rate of 0.002, 0.2, 2 and 20 per seconds. Clearly as strain rate increases, forming limit diagram increases upward. To compare, we can use minimum point of forming limit diagram that is representative of plane strain. As you can see in figure 4, in strain rate 2 per second, in minimum point of forming limit diagram, the maximum main strain is 0.3 which nearly equals the value of the point in dependent diagram to strain rate in figure 3. While in very low strain rate 0.002 per second, the maximum limit strain equals 0.2 that is the same of independent diagram to strain rate in figure 3. Dehra (2006) using experimental test on electromagnetic forming process showed increasing strain rate causes forming limit diagram increase. Obtained strain rate to experiment are put between 1 and 1000 per seconds.

Inhomogeneous in Forming Limit Diagram

By the definition of inhomogeneous' Hill 1948 in written algorithm, we can study this important parameter. Inhomogeneous coefficients are achieved using equation 20:

$$r = \frac{\varepsilon_W}{\varepsilon_T} \qquad (20)$$

Which in equation 20, ε_w and ε_t are strain along width and strain long thickness. Obtaining thickness of strain is so difficult, due to this, to principle of material volume being constant is used as equation:

$$\varepsilon_T = -(\varepsilon_W + \varepsilon_L) \qquad (21)$$

In equation 21, ε_l is strain along length. To study inhomogeneous effect on forming limit diagram, in addition to change in yield function, other parameters must be achieved such as hardening strain, strength coefficient power of sensitivity to strain rate in different directions respect to rolling. As a result, their average value is used as equation 22 (Hosford, 2007).

$$\bar{r} = \frac{r_0 + 2r_{45} + r_{90}}{4} \qquad (22a)$$

$$\bar{K} = \frac{K_0 + 2K_{45} + K_{90}}{4} \qquad (22b)$$

$$\bar{n} = \frac{n_0 + 2n_{45} + n_{90}}{4} \qquad (22c)$$

$$\bar{m} = \frac{m_0 + 2m_{45} + m_{90}}{4} \qquad (22e)$$

Putting this average value, we also studied inhomogeneous effect on forming limit diagram. Figure 5 shows inhomogeneous effect on forming limit diagram in strain rate 20 per second. As it is obvious, inhomogeneous changed surface of diagram.

Comparison

Metal sheet stainless steel 316 with thickness of 1 mm is put under forming process using drop hammer and all experimental stages are stimulated in Abaqus software and two criteria are entered to software: static and dynamic damage. Using static criterion of figure 3 and dynamic criterion of figure 4, figures 6 and 7 show simulation of this process. Value of damage parameter in both criteria is 0.709 and 0.861 that shows failure in sheet break. It is important to say that critical value of damage parameter in Abaqus

software equals 1 that shows break in sheet. Calculating damage parameter in Abaqus for all defined damage parameters is the same.

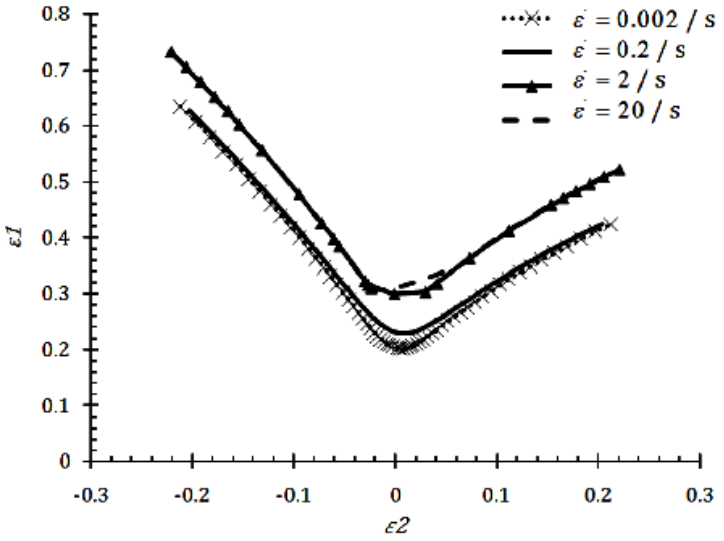

Figure 4: Dynamic Forming Limit Diagram of Stainless Steel 316

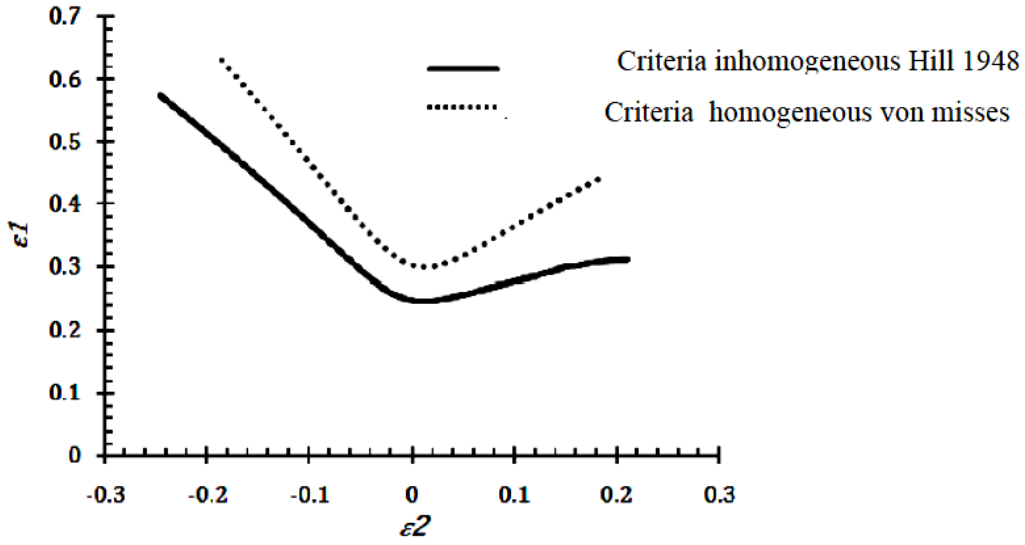

Figure 5: Inhomogeneous Effect on Forming Limit Diagram of Stainless Steel 316

Figure 8 shows how to calculate damage parameter D for damage criterion FLD defined in software. From equation 23, the damage parameter is calculating for this criterion:

$$D = \frac{\varepsilon_1^A}{\varepsilon_1^B} \qquad (23)$$

In equation 23, ε_1^A is main strain calculated by software along process, ε_1^B is main strain entered to software by damage criterion (figure 3). Calculating damage parameter for MSFLD criterion is the same of equation 23, too. If damage parameter D in equation 23 is reached the limit value 1, that element gets damaged completely and in that area, sheet gets broken. To better comparison, experiment is done on sheet with thickness of 0.8mm, figure 9 shows formed sheet which is broken. Figure 10 shows prediction of static damage criterion for stainless steel 316 in which critical damage parameter equals 0.745

indicating failure in sheet break. While figure 11 implies prediction of dynamic forming criterion in which damage parameter is reached critical value 1.

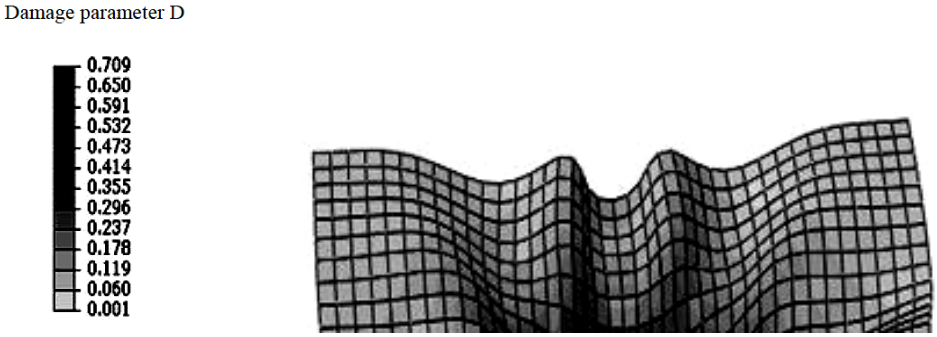

Figure 6: Predictive Result for Sheet with Thickness 1mm Using Static Criterion

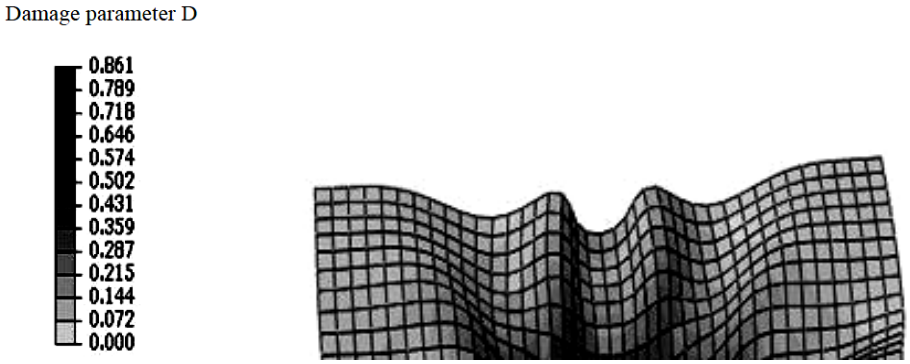

Figure 7: Predictive Result for Sheet with Thickness 1mm Using Dynamic Criterion

According to obtained results from experiment, it is concluded that static criterion can't exactly predict forming process and it implies effect of strain rate parameter that in this simulation is reached 20 per second and its effect on break is completely obvious. Same experiments are done for 3 pieces with thickness of 0.8 mm and three pieces with thickness of 1 mm and all experiment settings are put in software. To study accuracy of experiment using simulation, we can compare possible sheet break and depth of break in either experimented piece or simulation. For all three experimented pieces with thickness of 1mm, no break is occurred and in simulation, no break is observed. For all three experimented pieces with thickness of 0.8mm, the break is occurred in distance of 6mm from bottom of the piece. This experiment is done for three pieces in the same setting.

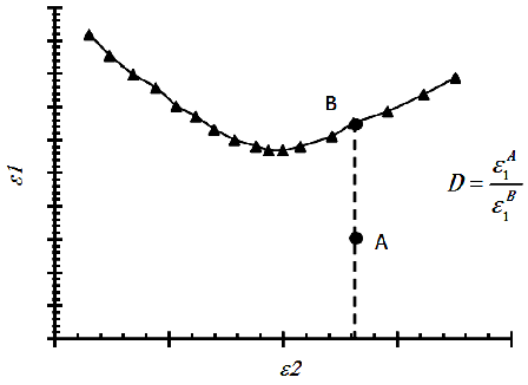

Figure 8: How to Calculate Critical Damage Parameter in Abaqus Software

Figure 9: Formed Sheet by Laser Assisted Forming with Thickness of 0.8 mm

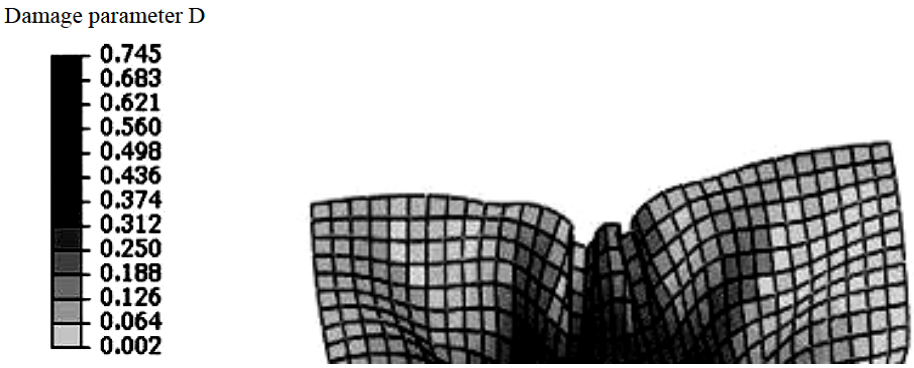

Figure 10: Predictive Result for Sheet with Thickness of 0.8 mm Using Static Criterion

To measure the place of break in simulation, we can account the number of sheet elements and can estimate place of break by knowing element's length.

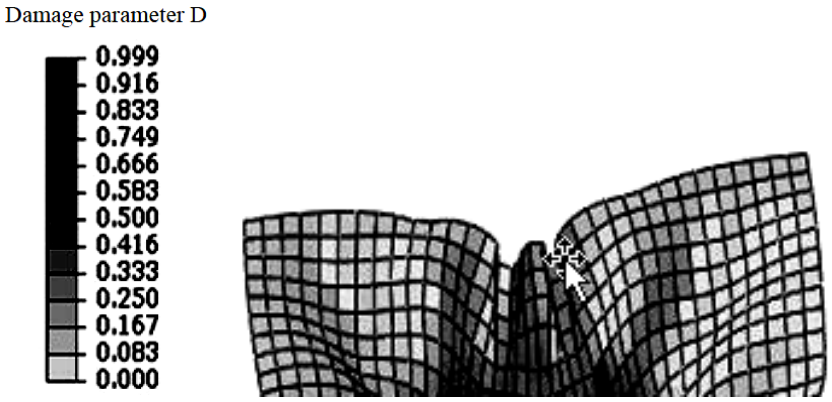

Figure 11: Predictive Result for Sheet with Thickness of 0.8 mm Using Dynamic Criterion

In meshing model, length of each element is determined 3 mm and according to this fact that there is three elements from bottom of the piece to the place of break, occurred break from bottom is 6mm that has a great compatibility with done experiment. Using element remove technique and enabling element remove option, we can tell software if calculated damage parameter in any element is reached one using equation 22, that element must be removed. Since estimating break is from bottom to the starting occurred break, also in simulation, we must account number of elements from bottom of the piece to the highest element which is broken.

Conclusion

We conclude that for problems having significant speed and strain rate, one can use static forming limit diagram. As in current article, this criterion for sheet with thickness of 0.8 mm causes incorrect prediction. Laser assisted forming process that is a common forming method with high speed, this method had a high error and is unable to predict damage exactly. For this kind of process, we must use dynamic forming limit diagram. We also concluded from this article that strain rate is an effective parameter on

material behavior and forming limit diagram of this material depends on strain rate. Therefore, if performed process has a high speed and the used material depends to strain rate, only exact criterion to predict damage correctly will be dynamic forming limit.

ACKNOWLEDGEMENT
We are grateful to Jam petrochemical company for their useful collaboration.

REFERENCES
Ahmadi S, Eivani AR and Akbarzadeh A (2009). Experimental and analytical studies on the prediction of forming limit diagrams. *Computational Materials Science* **44**(4) 1252-7.
Assempour A and Ganjiani M (2008). Implementation of a robust algorithm for prediction of Forming limit diagrams. *Journal of Materials Engineering and Performance* **17** 1-6.
Barata da Rocha A, Barlat F and Jalinear JM (1984). Prediction of the Forming Limit Diagram of Anisotropic Sheets in Linear and Non-linear Loading. *Materials Science and Engineering* 151-164.
Beria CH, Butuc MC, Gracio JJ, Rocha JE and Duarte JMF (2006). Theorical and Experimental Determination of forming limit diagram for AISI304 stainless steel. *Journal of Material Processing Technology* **179** 56-60.
G**oodwin GM (1969).** Application of Strain Analysis to Sheet Metal Forming Problems. *Metallurgia Italiana* **60** 767-771
Hosford W (2007). *Metal Forming Mechanics and Metallurgy*. In: Robert M.Caddell. *Plastic Anisotropy* 13.207-13.209.
Hosford W (2007). *Metal Forming Mechanics and Metallurgy*. In: Robert M.Caddell. (Cambridge University Press, Cambridge, UK).
Jie M, Cheng CH, Chan LC and Chow CL (2009). Forming Limit Diagrams of Strain-rate-dependent Sheet Metals. *International Journal of Mechanical Sciences* **51**(4) 269-275.
Kim SB, Huh H, Bok HH and Moon MB (2011). Forming Limit of Diagram of auto-body steel Sheets for high-speed Sheet Metal Forming. *Journal of Materials Processing Technology* **211**(5) 851-62.
Keeler SP (1965). Circular Grid System: A valuabe Aid for Evaluation Sheet Forming. *Sheet Metal Industries* 633-640.
Marciniak Z and Kuczynski K (1967). Limit Strains in the Process of Stretch Forming Sheet Metal. *International Journal of Mechanical Science* **9**(9) 609 IN1613-12IN2620.
Marciniak Z, Kuczynski K and Pokora T (1973). Influence of the Plastic Properties of a Material on the Forming Limit Diagram for Sheet Metal in Tension. *International Journal of Mechanical Science* **15**(10) 789-800.
Dehra MS (2006). High Velicity Formability and Factors Affecting it. *Tube Expansion Experiments* 99-111. Ohio United states
Moshksar MM and Mansorzadeh S (2003). Determination of the forming limit diagram for Al3105 sheet. *Journal of Materials Processing Technology* **141**(1) 138-142.
Sowerby R and Duncant JL (1971). Failure in Sheet Metal in Biaxial Tension. *International Journal of Mechanical Science* **13**(3) 217-229.